Meas. Sci. Technol. **19** (2008) 065305 (9pp) doi:10.1088/0957-0233/19/6/065305

Generation and spectroscopic application of tunable continuous-wave terahertz radiation using a dual-mode semiconductor laser

I Park[1,3], C Sydlo[2], I Fischer[1,4], W Elsäßer[1] and H L Hartnagel[2]

[1] Institute of Applied Physics, Darmstadt University of Technology, Schlossgartenstraße 7, D-64289 Darmstadt, Germany
[2] Institut für Hochfrequenztechnik, Darmstadt University of Technology, Merckstr. 25, D-64283 Darmstadt, Germany

E-mail: elsaesser@physik.tu-darmstadt.de

Received 6 September 2007, in final form 19 March 2008
Published 8 May 2008
Online at stacks.iop.org/MST/19/065305

Abstract
We present a tunable continuous-wave terahertz radiation source based on photomixing of a tunable dual-mode semiconductor laser on a log-periodic antenna. The discontinuously tunable dual-mode emission of the laser is achieved by spectrally filtered feedback in a double-external-cavity configuration. Two different two-frequency lasing regimes have been identified: pure dual-mode and dual-mode-comb emission. We spectrally investigate the laser emission in these two regimes and study the consequences for the generation of terahertz radiation. Under pure dual-mode emission, we achieve higher power, higher coherence and good tunability of the THz radiation. We demonstrate by detecting absorption lines of water vapor and hydrochloric acid gas that our concept for a tunable continuous-wave terahertz radiation source offers attractive properties for spectroscopic applications.

Keywords: tunable external cavity semiconductor laser, dual-mode operation, photomixing, tunable cw terahertz radiation, Fourier transform, spectroscopy

(Some figures in this article are in colour only in the electronic version)

1. Introduction

During the past two decades, the terahertz (THz) frequency region has attracted huge interest in science and technology. Numerous applications of THz systems have been demonstrated including imaging [1–4], nondestructive inspection [5] and security screening [6]. A major potential application of THz systems is in the spectroscopic analysis of many fundamental molecules. Various polar molecules exhibit characteristic absorption lines arising from pure rotational transitions in the THz frequency region. Chemical substances such as illegal drugs or explosives show their characteristic absorption spectra at THz frequencies [6, 7]. Therefore, many gases, gas mixtures and chemical substances can be monitored by sensing and identifying their absorption spectra via THz spectroscopy. Meanwhile, different pulsed and continuous-wave (CW) THz sources have been developed [8–14] and spectroscopic studies have been performed using THz time-domain spectroscopy [15–17] or CW THz systems [18–21]. However, compact and cost-effective CW THz sources that are coherent, tunable and operate at room temperature are still lacking. An attractive approach to realize such THz sources is photomixing of two optical laser modes from a tunable two-frequency semiconductor laser [22–25]. The concept of using a tunable two-frequency semiconductor laser as the optical source for photomixing allows a compact, cost-efficient configuration and wide frequency-tunability [26].

[3] Present address: Sacher-Lasertechnik, D-35037 Marburg, Germany.
[4] Present address: School of Engineering and Physical Science, Heriot-Watt University, Edinburgh EH14 4AS, UK.

Furthermore, the two-frequency laser allows an inherent spatial overlap of two laser frequencies and stable beat frequencies due to the common-mode rejection effect which is attributed to the compensation of the same fluctuations in the laser frequencies at the beat frequency [22]. Some concepts for two-frequency semiconductor lasers have been developed [27–32, 34, 35], very recently also one within a completely integrated concept [36]. However, achieving stability and spectral purity of dual-mode emission in long external cavities is still one of the open questions.

In this paper, we present a compact THz source using photomixing of two laser modes from a two-frequency semiconductor laser and demonstrate the generation of tunable CW THz radiation. To realize a two-frequency semiconductor laser we apply a concept employing a double-external-cavity configuration. We demonstrate two different regimes of two-frequency emission of the semiconductor laser, exhibiting two external cavity modes (pure dual-mode) or two external cavity combs (dual-mode-comb), respectively. The THz radiation performance for these two lasing regimes has been characterized. Our concept for the two-frequency semiconductor laser enables pure dual-mode emission, which allows the generation of coherent THz radiation with a narrow linewidth. Finally, we employ our THz source for spectroscopic applications and identify absorption spectra of water vapor and hydrochloric acid (HCl) gas.

The method of photomixing is based on the difference frequency mixing (or optical heterodyne downconversion) of two linearly polarized CW laser beams with angular frequencies ω_1 and ω_2 on a photoconductive device. The photoconductive device consists of a semiconductor material with a short carrier lifetime (<1 ps), such as low-temperature grown gallium arsenide (LT-GaAs), and an antenna, which acts as a THz emitter. When two laser beams are incident on the photoconductive material, the conductance of the material is modulated with the difference frequency of the two beams. The incident power can be described by

$$P(t) = P_1 + P_2 + 2\sqrt{mP_1P_2}\cos\omega t, \tag{1}$$

where $\omega = \omega_1 - \omega_2$ is the angular frequency difference of two laser beams with average powers P_1 and P_2, respectively, and m is the mixing efficiency depending on the spatial overlap of the incoming beams. Here, the terms that vary with higher frequencies than ω are neglected because the photoconductor cannot respond to such rapid variation with a timescale much shorter than the photocarrier lifetime of the photoconductor. When a bias voltage is applied to the photomixer, the photocurrent is modulated at the difference frequency ω [18, 37], that is,

$$I(t) = I_0\left(1 + \frac{2\sqrt{mP_1P_2}\sin(\omega t + \phi)}{P_0\sqrt{1+\omega^2\tau^2}}\right), \tag{2}$$

where $I_0 = \eta_e(e/h\nu)P_0$ is the dc photocurrent, $P_0 = P_1 + P_2$ is the averaged total incident power, τ is the carrier lifetime of the photoconductive material, ϕ denotes a phase shift which depends on carrier lifetime, e is the electron charge, $h\nu$ is the photon energy and η_e indicates the external quantum efficiency of converting the optical signal incident on the photomixer to an electrical signal. Driven by the modulated photocurrent, an electromagnetic wave at frequency ω is radiated from the antenna into free space.

The generated THz radiation output power $P_{THz}(\omega)$ is given in the small-signal limit by [37]

$$P_{THz}(\omega) = 2(I_0)^2 R_A \frac{mP_1P_2}{P_0^2[1+(\omega\tau)^2][1+(\omega R_A C)^2]}, \tag{3}$$

R_A is the radiation resistance of the antenna and C is the capacitance of the photoconductive gap. The frequency performance of the THz emitter is limited by τ and the R_AC time constant. In the following sections, we show the experimental approach and results for the dual-mode emission of the laser and the generation of tunable CW THz radiation. Finally, we demonstrate spectroscopic applications of the THz source for sensing absorption lines of sample gases.

2. Experimental setup

The experimental setup of the tunable CW THz system is shown in figure 1. As an optical laser source for photomixing we have developed a tunable two-frequency semiconductor laser using a double-external-cavity configuration (2λ-ECSL) [35]. Our 2λ-ECSL is depicted in the dotted box in figure 1. The laser system consists of a semiconductor laser, an antireflection-coated aspheric collimation lens, a diffraction grating (1200 lines mm^{-1}), a 50/50 beam splitter and two high-reflective mirrors M1 and M2. A commercial index-guided, multiple-quantum-well (MQW) semiconductor laser (GaAlAs, Hitachi) with a central wavelength of 785 nm, a maximum output power of 50 mW and a geometric cavity length of 670 μm is used as a gain medium. The laser has a high-reflective rear facet and a low-reflective front facet. The laser is thermally stabilized at room temperature. The laser beam from the front facet is collimated by the aspheric lens and is directed onto the diffraction grating. The first-order diffraction beam of the grating is coupled into the external double-cavity. The beam is divided into two beams by a beam splitter, each of which is directed into each branch of the cavity. Within each branch of the cavity, the selection of the desired wavelength is performed by spectrally selected feedback of the laser beam via tilting the external mirror and simultaneously moving the mirror along the beam direction. The total external cavity length amounts to 17 cm. Since the output facet of the laser has a residual reflectivity, only external cavity modes which are resonant with the solitary laser modes will be effectively amplified, defining the compound cavity modes. Therefore, our THz source can only be tuned discontinuously in steps of 63 GHz. The zeroth-order grating beam is coupled out as output beam and is sent through an optical isolator to a beam splitter. The beam splitter extracts a small portion of the incident light which is used to monitor the optical spectrum of the laser light by an optical spectrum analyzer (OSA) with a resolution of 0.05 nm and a scanning Fabry–Perot (FP) interferometer with a free spectral range (FSR) of 10 GHz and a resolution of 50 MHz. The main beam is chopped by a chopper and is then focused by an aspheric lens on the pre-biased photomixer on the LT-GaAs chip. We used

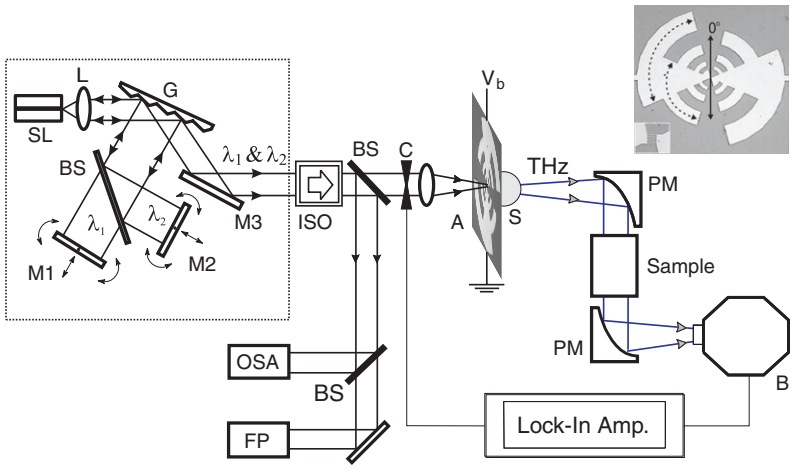

Figure 1. Experimental setup. SL: semiconductor laser; L: lens; BS: beam splitter; G: grating; M1, M2: external mirrors; M3: mirror for output coupling; ISO: optical isolator; OSA: optical spectrum analyzer; FP: Fabry–Perot interferometer; C: chopper; A: log-periodic antenna; S: silicon lens; PM: parabolic mirror; B: bolometer. The photograph in the right corner shows the log-periodic antenna.

a log-periodic circular-toothed planar antenna. The antenna is fabricated on a 600 nm thick LT-GaAs by lithography grown on 400 nm GaAlAs on a semi-insulating GaAs substrate. The photomixer in the feedpoint of a log-periodic circular-toothed planar antenna consists of six 1 μm wide interdigitated electrode fingers with gaps of 1 μm between each of them. The fingers are 9 μm long such that the photomixer has an area of 10 μm by 11 μm. The antenna and the finger consist of 100 nm thick platinum directly evaporated on the LT-GaAs. The log-periodic circular-tooth antenna has an outer radius of 640 μm with a ratio of the edge distance of successive teeth of 0.5 and the tooth width being square root of 0.5. There are three teeth either side of the bow-tie shape with an angle sustained by teeth and bow-tie of 50°. The innermost portion has a bow-tie shape with an angle of 100°. A photograph of the antenna structure is shown at the right corner of figure 1. The characteristics of this THz emitter are described in [38, 39].

The generated THz radiation is coupled out into free space through a hyperhemispherical high-resistivity silicon lens which is attached to the backside of the antenna chip. The THz radiation is then collimated by an off-axis parabolic mirror and another parabolic mirror is used to focus the collimated THz radiation directly onto a silicon bolometer cooled to 4 K. The output of the bolometer is measured with a lock-in amplifier. A Fourier-transform spectrometer (FTS) has been used for the spectral characterization of the generated radiation. In addition, a sample cell with a length of 8 cm made of 1 mm thick polyethylene (PE) can be inserted into the collimated THz beam for gas sensing.

3. Results and discussion

3.1. Generation of THz radiation exploiting two different two-frequency lasing regimes

To characterize and optimize the generation of THz radiation, we have analyzed the optical spectra of the two-frequency laser beam by the OSA and the scanning FP interferometer in order to resolve the modes of the solitary semiconductor laser chip and the external cavity, respectively. Simultaneously, we have spectroscopically investigated the generated THz radiation using the FTS. The laser was driven at a constant injection current of 187 mA. Accordingly, the average power of the laser light incident on the photomixer was 12 mW. The antenna was biased at a voltage of 15 V.

Firstly, we have investigated the characteristics of the two-frequency emission of the semiconductor laser. Figure 2 shows optical spectra for two two-frequency emission regimes of the semiconductor laser. The first regime displayed in figure 2(*a*) shows an optical spectrum of the laser emission in which the two laser modes and a weak four-wave mixing (FWM) sideband can be identified. The wavelengths of the modes are 784.14 nm and 785.98 nm, respectively, corresponding to a difference frequency of 896 GHz. The simultaneous spectral scan by the FP interferometer monitors the spectral purity of the two-frequency operation with a resolution of about 60 MHz. As shown in figure 2(*b*), the laser emits only two external cavity modes which appear as clear peaks with comparable intensity in the FP scan. The linewidth of each mode cannot be resolved with the used FP, therefore being smaller than 60 MHz. Since the external cavity modes have a mode spacing of about 880 MHz corresponding to the external cavity length, the FP scan should reveal any possible modes, if the laser beam contained additional external cavity modes. In this regime the total intensity exhibits a simple modulation pattern which corresponds to the interference of the two modes. The difference frequency should then only exhibit one frequency component with a narrow linewidth without any other frequency components. This regime is that which we define as the pure dual-mode lasing regime.

Another type of two-frequency lasing regime is shown in figures 2(*c*) and (*d*). An optical spectrum recorded by the OSA shown in figure 2(*c*) displays two spectrally separated laser modes and a weak FWM sideband, as for the case of figure 2(*a*). The difference wavelength of the modes amounts

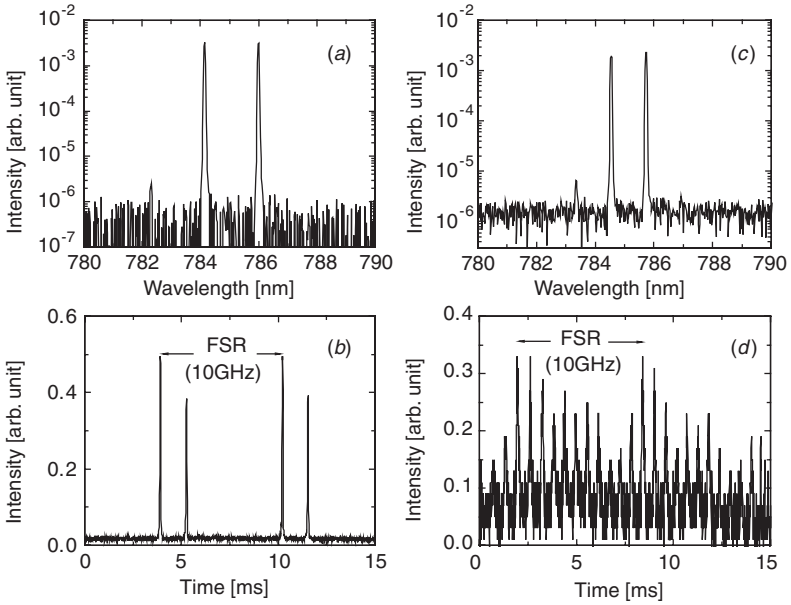

Figure 2. Two regimes of two-frequency emission: (*a*) and (*c*) are optical spectra recorded by OSA. (*b*) and (*d*) are Fabry–Perot-interferometer scans corresponding to (*a*) and (*c*), respectively.

to 1.2 nm which corresponds to a difference frequency of 584 GHz. From the OSA spectrum one could initially suppose that the laser oscillates in the pure dual-mode regime. However, a high-resolution spectrum recorded simultaneously by the FP interferometer depicted in figure 2(*d*) shows that these spectral peaks consist of several external cavity longitudinal modes (external mode-comb) with a mode spacing of 880 MHz. The width of each external mode-comb amounts to about 3.5 GHz. These two external cavity mode-combs are characteristic of the two-frequency lasing regime which is usually achieved in a long external cavity configuration [34]. In this regime the total intensity exhibits a complex intensity modulation caused by interference among several external cavity modes, which should exhibit several different frequency components.

The transition between these two different operation regimes requires proper, reliable and well-defined control of the cavity conditions. The total length of the double Littman configuration amounts to 17 cm which is equivalent to a frequency mode spacing (in air) of 880 MHz, whereas the total length of the semiconductor laser amounts to 670 μm resulting in a mode spacing (with a refractive index of 3.5) of 63 GHz. These two mode frequencies together with the feedback conditions govern the type of modal emission, either dual mode or dual mode-comb emission. Due to the fact that the semiconductor laser chip has a non-zero residual reflectivity (in the order of some per cent in our case) only discontinuous tuning behavior is possible. In order to suppress the solitary modes (i.e. those of the short semiconductor laser chip) AR-coatings with reflectivities below 10^{-4} or 10^{-5} are requested. Therefore, careful matching of the solitary (short) cavity modes with those of the (long) external cavity modes, accompanied by piezo-precise angle tuning of the grating, is the experimental necessity.

However, looking also to theory [34] we can even deduce eventually a further strategy to achieve this coherent single dual operation and relate it to our experimental realization. Eventually, it is just this non-perfect AR-coating which works in supporting the pure dual-mode operation. The residual reflectivity of the semiconductor laser Fabry–Perot cavity acts on the one hand as a narrow-band filter which allows the suppression of more external cavity modes, if not being in perfect resonance, thus enabling the achievement of the coherent regime [34] where this possible or necessary filter effect has also been requested or deduced theoretically. This will be the subject of further investigations. In conclusion, we have been able to establish pure dual-mode emission of the laser by a careful matching of the solitary (short) cavity modes to those of the (long) external cavity modes. This fine cavity adjustment has been performed with an angle tuning of the grating accompanied via a coarse micrometer tuning and a precise piezo tuning. Since the external mode spacing increases with decreasing external cavity length, the stability of the pure dual-mode emission can be further improved with a compact external cavity configuration.

Secondly, we have investigated the characteristics of the generated THz radiation for both two-frequency lasing regimes. Figure 3 shows interferograms and spectra of the generated THz radiation obtained by the FTS measurements, which correspond to the optical spectra in figure 2. A recorded FTS interferogram of the generated THz radiation for the pure dual-mode lasing regime is shown in figure 3(*a*) as a function of the optical path difference up to 4.6 cm, the maximum realized delay in the FTS for this case. The signal shows a more or less constant modulation of the intensity with increasing optical path difference. The slow variation of the maximum intensities in figure 3(*a*) results from slight variations of the relative power of the laser modes in time.

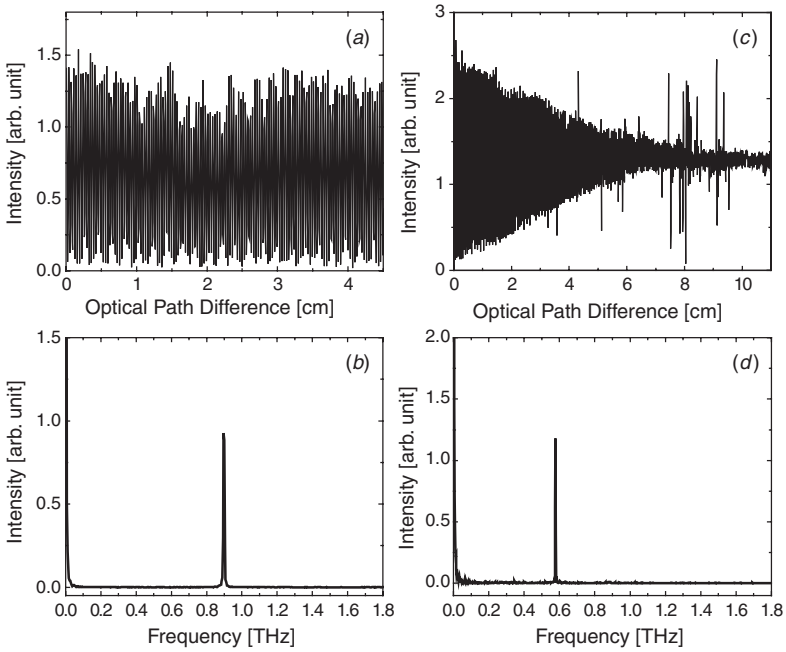

Figure 3. The generated THz radiation corresponding to the two regimes of two-frequency emission of figure 2: (*a*) and (*c*) are interferograms of the generated THz radiation measured with FTS. (*b*) and (*d*) are fast Fourier transforms of the interferograms corresponding to (*a*) and (*c*), respectively.

The decrease (increase) in optical intensity modulation due to the increase (decrease) in the optical power difference between both laser modes results in a decrease (increase) of the generated THz power. The variation of the THz power results in a variation of the maximum intensity of the interferogram. The fast Fourier transform (FFT) of the recorded interferogram is shown in figure 3(*b*). The FFT shows THz radiation at a single frequency of 896 GHz which is the same as the difference frequency of the two laser modes recorded with the OSA. The linewidth of the THz radiation is measured to be approximately 7 GHz, which is resolution-limited due to the spectral resolution of the FTS of 6.5 GHz corresponding to the used maximum path difference of 4.6 cm. However, by fitting the visibility of the interferogram with an exponentially decaying function with a coherence length of 800 cm [22], we are able to estimate the linewidth of the THz radiation to be about 40 MHz . Due to this high coherence, the pure dual-mode lasing regime is the desirable case for generation of highly coherent THz radiation.

For the dual-mode-comb lasing regime, an interferogram of the generated THz radiation recorded by FTS measurement is shown in figure 3(*c*). The intensity modulation of the interferogram decreases symmetrically around the average intensity with increasing optical path difference. The maximum path difference investigated here is up to 11 cm and corresponds to a spectral resolution of 2.7 GHz. The decreasing behavior of the intensity modulation originates from the fact that the spectrally broad THz radiation due to the multiple external cavity modes results in a reduced coherence length of the radiation. The FFT spectrum of this interferogram shows THz radiation at a single frequency of 578 GHz in figure 3(*d*). The THz radiation frequency is in good agreement with the beat frequency of 584 GHz of the two main laser peaks. The slight difference between the difference frequency recorded by the OSA and the THz frequency determined by the FTS measurement is due to the limited wavelength resolution of the used OSA. The measured linewidth of the THz radiation can be resolved by the FTS measurement and amounts to approximately 4 GHz which is smaller than the convolution of the 3.5 GHZ mode-comb widths due to the 'common mode rejection' of the correlated fluctuations. The linewidth in figure 3(*d*) is narrower than that in figure 3(*b*) because the spectral resolution of FTS measurement for figure 3(*d*) is higher than for figure 3(*b*). It is expected that the generated THz radiation at 578 GHz should contain several peaks with a frequency spacing of 880 MHz. However, they could not be resolved in the FFT spectrum due to the limited spectral resolution of the FTS.

The photomixing for the case of dual-mode-comb operation comprising several external cavity modes also allows the generation of THz radiation, providing a linewidth of the order of GHz. However, the THz radiation power so generated is not as high as in the case of the pure dual-mode lasing regime. In particular, for the same optical power in both cases, the power of the generated THz radiation for the dual-mode-comb operation reaches at maximum 20% of that for the pure dual-mode operation. The reduction of the generated THz radiation power for the dual-mode-comb operation can be explained by the combined interference among several external cavity modes. This is in contrast to the simple harmonic modulation in the case of the pure dual-mode superposition. Therefore, the time averaged total intensity modulation for the dual-mode-comb operation at the THz frequency is lower than in the pure dual-mode operation, and the power of the generated

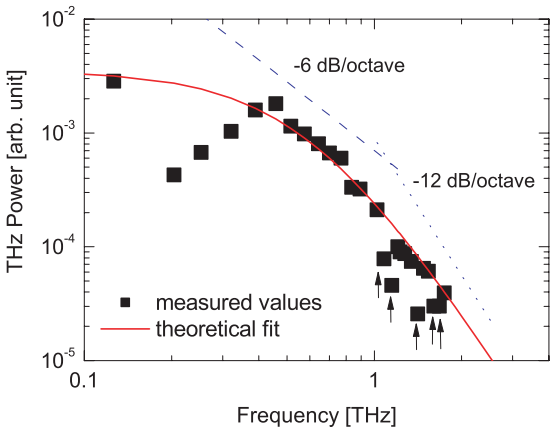

Figure 4. Spectral THz power emitted by the log-periodic antenna. Full squares represent measured values and the solid line represents the theoretical curve according to equation (3). The dashed and dotted lines show the roll-off of −6 dB/octave and −12 dB/octave, respectively.

THz radiation is reduced. Most of the power is emitted as radiation in the microwave frequency region corresponding to difference frequencies between several external cavity modes, thus lacking in THz power. As a result, a pure dual-mode laser source is desirable for the efficient generation of THz radiation. However, the dual-mode-comb laser source could be employed for less stringent generation of THz radiation which may well be used for many applications such as THz imaging. The following investigations have been performed in the pure dual-mode lasing regime.

3.2. *Spectral power of THz radiation*

The antenna converts the oscillation of electrical current with THz frequency in the photomixer into an electromagnetic wave coupled out to propagate in free space. Therefore, the power of the generated THz radiation exhibits characteristics of the antenna. The achievable frequency range of the THz radiation is determined by the bandwidth of the antenna. We present in this section the frequency dependence of the THz generation at a constant bias voltage of 18 V and an average incident optical power of 11 mW on the photomixer. The difference frequency of the two laser modes has been varied from 126 GHz to 1.8 THz.

The experimentally obtained THz power and the theoretical fit according to equation (3) with $R_A = 65\ \Omega$ and $C = 3$ fF are displayed in figure 4 as a function of the difference frequency of the laser modes. The experimental data (full squares in figure 4) show a dip at 204 GHz and increase with increasing frequency up to 457 GHz. Thereafter, they decrease with increasing frequency at a rate of −6 dB/octave (dashed line in figure 4) up to about 800 GHz and at a rate approaching −12 dB/octave (dotted line in figure 4) at higher frequencies larger than 1 THz. The detected THz power at the maximum of figure 4 at a frequency of 457 GHz corresponds to 0.160 nW.[5] The theoretical values (solid line in figure 4) show behavior which decreases slowly with increasing frequency up to about 400 GHz and thereafter similar decreasing behavior as that of the measured data. The measured data above 400 GHz agree well with the theoretical results. The decrease in radiation power with increasing frequency is attributed to the bandwidth limitation via the carrier lifetime and the capacitance of the photomixer. The finite lifetime required for the excited carriers in the photoconductive material to recombine efficiently limits the performance of the device as the frequency increases. In addition, since the region of the interdigitated electrode fingers possesses a capacitance, the capacitance affects the behavior of the photomixer in the THz frequency range and causes the antenna impedance to short-cut at high frequencies. The roll-off in the frequency performance at the rate of −6 dB/octave in figure 4 is due to the carrier lifetime. From the theoretical fit to the measured data, the carrier lifetime in the LT-GaAs material can be estimated by equation (3), resulting in a value of 350 fs. This value is in good agreement with the value determined by a pump-and-probe measurement [40]. An additional $R_A C$ time constant of 195 fs which is given by $R_A = 65\ \Omega$ and $C = 3$ fF limits the frequency performance with a roll-off rate of −6 dB/octave [38]. Thus, the high-frequency roll-off at the rate of −12 dB/octave in figure 4 is due to the combination of the carrier lifetime and the $R_A C$ time constant. In further investigations we have ascertained that the used antenna can be operated up to 2.8 THz.

The difference of the behavior shown at frequencies below 400 GHz can be attributed to the antenna characteristics not accounted for in equation (3). Since the log-periodic toothed antenna shows a periodic resonance behavior, there are alternating low and high generation efficiencies of THz radiation depending on the THz frequency. Our theoretical calculation does not take these periodic characteristics into consideration. The differences in the high-frequency region indicated by arrows at frequencies 1.08, 1.148, 1.41, 1.606 and 1.674 THz are attributed to the absorption of THz radiation by water vapor in the atmosphere [41, 42]. In the following section we study how far our THz source can be utilized for spectroscopic applications.

3.3. *Spectroscopic application*

Our tunable THz radiation source finds its potential application in spectroscopy of gases. To demonstrate the capability of the source for such an application, we have applied our THz source to sense absorption lines of sample gases. This has been realized by measuring the spectral transmission of THz radiation through a gas-filled cell. The THz system is driven at the same conditions as in the previous section. We have used water vapor and HCl gas as sample gases. These are polar molecules with well studied spectral lines

[5] We have to state that this number for the THz power has been directly obtained via the bolometer response without particular emphasis either on particularly optimized off-axis paraboloids or special THz lenses or beam shaping optics in front of the bolometer. This underlines the excellent signal-to-noise ratio of our set-up which is equally important for the application to spectroscopy experiments.

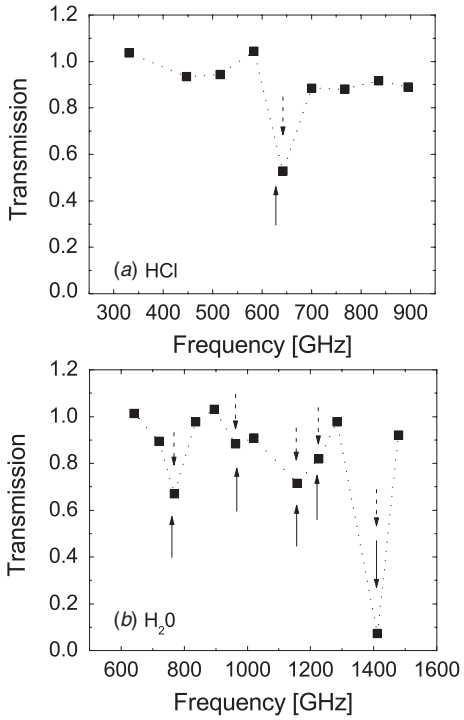

Figure 5. Spectral transmission of THz radiation through (*a*) HCl in gas phase and (*b*) water vapor. The solid arrows represent known absorption lines according to [41] and the dashed arrows indicate frequencies with relatively low THz transmission in experiment. The dotted lines are guides to the eye. The error bars in the spectral transmission amount to approximately 0.05

in the THz frequency range [15, 16, 41–44]. Commercial polyethylene square bottles with a wall-thickness of about 1 mm are used as sample cells for the gases due to their well-known transparency for THz radiation [17]. The bottles are first filled with N_2 gas to purge any other molecules from them and then either with HCl gas or water vapor. Thus, the sample bottles contain a mixture of N_2 and sample gases. As a reference, we have used an identical bottle filled with N_2 gas only. All gases in the bottles are at room temperature and atmospheric pressure. For the transmission measurements the bottles containing the samples are placed in the path of the THz radiation between two parabolic mirrors separated at a distance of about 14 cm, as shown in figure 1. The transmitted radiation is detected by the bolometer. The measured power of the THz radiation transmitted through the sample gases is normalized with respect to the power transmitted through the reference gas. Thus, we obtain the transmission through the sample gas, compensating for the influence of the bottle.

As a first example, we have used our THz source to identify the absorption line of HCl molecules in the frequency range between 300 GHz and 900 GHz. Here, the studied HCl gas contains $^1H^{35}Cl$ whose rotational absorption line lies at a frequency of 626 GHz (indicated by the solid arrow in figure 5(*a*)) [41, 43]. The measured spectral transmission for HCl gas is shown in figure 5(*a*). The measured data show a complete transmission of the THz radiation through the HCl gas in the frequency range between 300 and 900 GHz, except one dip at 642 GHz (indicated by the dashed arrow in the figure). The measured spectral line agrees well with that of $^1H^{35}Cl$ within a discrepancy of +16 GHz, corresponding to +2.5%. The uncertainty arising from the limited spectral resolution of the OSA of ±50 pm for determining the difference frequency of the two laser modes results in a frequency uncertainty of ±24 GHz for the THz signal. In addition, our THz source can only be tuned discontinuously in steps of 63 GHz due to compound cavity effects discussed previously. This discontinuous tuning step gives an additional uncertainty of ±31.5 GHz for resolving an absorption line. Thus, our system provides a total uncertainty of about ±40 GHz, which is our limitation in identifying correctly the absorption line of the HCl gas [45].

As a second example and to demonstrate the capability of our THz system for identification of several transition lines of a given element, we have measured transmission of water vapor in the frequency range between 600 GHz and 1.5 THz. Water vapor has many absorption lines in this THz range. The recorded spectral transmission is displayed in figure 5(*b*). The measured data show relatively low transmission at frequencies of 768 GHz, 962 GHz, 1.157, 1.225 and 1.412 THz (marked with dashed arrows in the figure), compared to data at other frequencies which show complete transmission. The frequencies with low transmission agree well with the rotational transition spectra of water vapor at 752 GHz, 970 GHz, 1.229 and 1.411 THz (marked with solid arrows in the figure) [15, 41, 42, 46]. The measured spectral lines in the present investigation agree with the expected lines within an error of about ±2%. For the measured line at 1.157 THz, we cannot clearly assign it to one particular frequency, since there are several rotational transitions at 1.153, 1.158 and 1.163 THz within the uncertainty of our measurement. For a clear identification of such closely lying absorption lines, it is desirable that the difference frequency of the two laser modes should be continuously tunable. Our system has discrete tuning steps of 63 GHz corresponding to the mode spacing of the solitary laser's Fabry–Perot cavity. The problem of the discrete tunability of our system could be circumvented by better antireflection coating on the laser facet which would allow a better quasi-continuous tuning of the laser modes.

4. Conclusion

We have demonstrated a tunable CW THz radiation system in which we have employed the photomixing method using a frequency-tunable dual-mode semiconductor laser. To realize a tunable dual-mode semiconductor laser we have employed a double-external-cavity configuration. We have identified two regimes of dual-mode emission of the laser in a long external cavity configuration—pure dual-mode and dual-mode-comb emission, respectively. We could achieve tunable pure dual-mode emission of the laser under a delicate control of frequency tuning and external cavity length. The stability of the pure dual-mode emission can be improved with a compact external cavity configuration. We have been able to generate THz radiation in both lasing regimes. The generated THz

radiation for the pure dual-mode emission exhibits narrower linewidth and higher output power than for the dual-mode-comb emission. For spectroscopic demonstrations, we have successfully identified absorption lines of water vapor and HCl gas. Our results demonstrate that our concept for the THz radiation system, preferably with better antireflection coating on the laser facet and more compact external cavity configuration, provides an attractive source for generating continuously tunable, stable CW THz radiation.

Acknowledgments

This work has been supported by the Deutsche Forschungsgemeinschaft.

References

[1] Hu B B and Nuss M C 1995 Imaging with terahertz waves *Opt. Lett.* **20** 1716–8

[2] Siebert K, Quast H, Leonhardt R, Löffler T, Thomson M, Bauer T and Roskos H G 2002 Continuous-wave all-optoelectronic terahertz imaging *Appl. Phys. Lett.* **80** 3003–5

[3] Löffler T, May T, am Weg C, Alcin A, Hils B and Roskos H G 2007 Continuous-wave terahertz imaging with a hybrid system *Appl. Phys. Lett.* **90** 091111–1

[4] Gregory I S, Tribe W R, Baker C, Cole B E, Evans M J, Spencer L, Pepper M and Missous M 2005 Continuous-wave terahertz system with a 60 dB dynamic range *Appl. Phys. Lett.* **86** 204104–1

[5] Karpowicz N, Zhong H, Xu J, Lin K-I, Hwang J-S and Zhang X-C 2005 Comparison between pulsed terahertz time-domain imaging and continuous wave terahertz imaging *Semicond. Sci. Technol.* **20** S293–9

[6] Federici J F, Schulkin B, Huang F, Gary D, Barat R, Oliveira F and Zimdars D 2005 THz imaging and sensing for security applications—explosives, weapons and drugs *Semicond. Sci. Technol.* **20** S266–80

[7] Kawase K, Ogawa Y and Watanabe Y 2003 Non-destructive terahertz imaging of illicit drugs using spectral fingerprints *Opt. Exp.* **11** 2549–54

[8] Auston D H, Cheung K P and Smith P R 1984 Picosecond photoconducting Herzian dipoles *Appl. Phys. Lett.* **45** 284–6

[9] Xu L, Zhang X-C and Auston D H 1992 Terahertz beam generation by femtosecond optical pulses in electro-optic materials *Appl. Phys. Lett.* **61** 1784–6

[10] Zhang X-C, Hu B B, Darrow J T and Auston D H 1990 Generation of femtosecond electromagnetic pulses from semiconductor surfaces *Appl. Phys. Lett.* **56** 1011–3

[11] Brown E R, McIntosh K A, Nichols K B and Dennis C L 1995 Photomixing up to 3.8 THz in low-temperature-grown GaAs *Appl. Phys. Lett.* **66** 285–7

[12] Köhler R, Tredicucci A, Beltram F, Beere H E, Linfield E H, Davies A G, Ritchie D A, Iotti R C and Rossi F 2002 Terahertz semiconductor-heterostructure laser *Nature* **417** 156–9

[13] Kawase K, Shikata J-I, Imai K and Ito H 2001 Transform-limited, narrow-linewidth, terahertz-wave parametric generator *Appl. Phys. Lett.* **78** 2819–21

[14] Hoffmann S *et al* 2004 Four-wave mixing and direct terahertz emission with two-color semiconductor lasers 2004 Four-wave mixing and direct terahertz emission with two-color semiconductor lasers *Appl. Phys. Lett.* **84** 3585–7

[15] van Exter M, Fattinger Ch and Grischkowsky D 1989 Terahertz time-domain spectroscopy of water vapor *Opt. Lett.* **14** 1128–30

[16] Mittleman D M, Jacobsen R H, Neelamani R, Baraniuk R G and Nuss M C 1998 Gas sensing using terahertz time-domain spectroscopy *Appl. Phys.* B **67** 379–90

[17] Ikeda T, Matsushita A, Tatsuno M, Minami Y, Yamaguchi M, Yamamoto K, Tani M and Hangyo M 2005 Investigation of inflammable liquids by terahertz spectroscopy *Appl. Phys. Lett.* **87** 034105–1

[18] Pine A S, Suenram R D, Brown E R and McIntosh K A 1996 A terahertz photomixing spectrometer: application to SO_2 self broadening *J. Mol. Spectrosc.* **175** 37–47

[19] Matsuura S, Tani M, Abe H, Sakai K, Ozeki H and Saito S 1998 High-resolution terahertz spectroscopy by a compact radiation source based on photomixing with diode lasers in a photoconductive antenna *J. Mol. Spectrosc.* **187** 97–101

[20] Mouret G, Matton S, Bocquet R, Hindle F, Peytavit E, Lampin J F and Lippens D 2004 Far-infrared cw difference-frequency generation using vertically integrated and planar low temperature grown GaAs photomixers: application to H_2S rotational spectrum up to 3 THz *Appl. Phys.* B **79** 725–9

[21] Gregory I S, Tribe W R, Cole B E, Baker C, Evans M J, Bradley I V, Linfield E H, Davies A G and Missous M 2004 Phase sensitive continuous-wave THZ imaging using diode lasers *Electron. Lett.* **40** 143–4

[22] Gu P, Tani M, Hyodo M, Sakai K and Hidaka T 1998 Generation of cw-terahertz radiation using a two-longitudinal-mode laser diode *Japan. J. Appl. Phys.* **37** L976–8

[23] Gu P, Chang F, Tani M, Sakai K and Pan C-L 1999 Generation of coherent cw-terahertz radiation using a tunable dual-wavelength external cavity laser diode *Japan. J. Appl. Phys.* **38** L1246–8

[24] Kleine-Ostmann T, Knobloch P, Koch M, Hoffmann S, Breede M, Hofmann M, Hein G, Pierz K, Sperling M and Donhuijsen K 2001 Continuous wave THz imaging *Electron. Lett.* **37** 1461–3

[25] Hoffmann S, Hofmann M, Kira M and Koch S W 2005 Two-colour diode lasers for generation of THz radiation *Semicond. Sci. Technol.* **20** S205–10

[26] Huang C-C, Cheng C-H, Su Y-S and Lin C-F 2004 174-nm mode spacing in a dual-wavelength semiconductor laser using nonidentical InGaAsP quantum wells *IEEE Photon. Technol. Lett.* **16** 371–3

[27] Wang C-L and Pan C-L 1994 Tunable dual-wavelength operation of a diode array with an external grating-loaded cavity *Appl. Phys. Lett.* **64** 3089–91

[28] Ito S, Suehiro M, Hirata T and Hidaka T 1995 Two-longitudinal-mode laser diodes *IEEE Photon. Technol. Lett.* **7** 959–61

[29] Pajarola S, Guekos G and Mørk J 1996 Optical generation of millimeter-waves using a dual-polarization emission external cavity diode laser *IEEE Photon. Technol. Lett.* **8** 157–9

[30] Lin C-F, Chen M-J and Lee B-L 1998 Wide-range tunable dual-wavelength semiconductor laser using asymmetric dual quantum wells *IEEE Photon. Technol. Lett.* **10** 1208–10

[31] Struckmeier J, Euteneuer A, Smarsly B, Breede M, Born M, Hofmann M, Hildebrand L and Sacher J 1999 Electronically tunable external-cavity laser diode *Opt. Lett.* **24** 1573–4

[32] Brunner M, Gulden K, Hövel R, Moser M, Carlin J F, Stanley R P and Ilegems M 2000 Continuous-wave dual-wavelength lasing in a two-section vertical-cavity laser *IEEE Photon. Technol. Lett.* **12** 1316–8

[33] Rogister F, Sukow D W, Gavrielides A, Mégret P, Deparis O and Blondel M 2000 Experimental demonstration of

suppression of low-frequency fluctuations and stabilization of an external-cavity laser diode *Opt. Lett.* **25** 808–10
[34] Matus M, Kolesik M, Moloney J V, Hofmann M and Koch S W 2004 Dynamics of two-color laser systems with spectrally filtered feedback *J. Opt. Soc. Am.* B **21** 1758–71
[35] Park I, Fischer I and Elsäßer W 2004 Highly nondegenerate four-wave mixing in a tunable dual-mode semiconductor laser *Appl. Phys. Lett.* **84** 5189–91
[36] Osborne S, O'Brien S, Buckley K, Fehse R, Patchell J, Kelly B, O'Gorman J and O'Reilly E P 2007 Two-colour Fabry–Perot laser with terahertz primary mode spacing *Electron. Lett.* **43** 224–5
[37] Brown E R, Smith F W and McIntosh K A 1993 Coherent millimeter-wave generation by heterodyne conversion in low-temperature-grown GaAs photoconductors *J. Appl. Phys.* **73** 1480–4
[38] Mendis R, Sydlo C, Sigmund J, Feiginov M, Meissner P and Hartnagel H L 2004 Tunable CW-THz system with a log-periodic photoconductive emitter *Solid-State Electron.* **48** 2041–5
[39] Mendis R, Sydlo C, Sigmund J, Feiginov M, Meissner P and Hartnagel H L 2005 Spectral characterization of broadband THz antennas by photoconductive mixing: toward optimal antenna design *IEEE Antennas Wirel. Propag. Lett.* **4** 85–8
[40] Lisauskas A 2006 private communication, Physikalisches Institut, Johann Wolfgang Goethe-Universität
[41] http://www.cfa.harvard.edu/hitran
[42] Möller K D and Rothschild W G 1971 *Far-Infrared Spectroscopy* (New York: Wiley)
[43] Klaus Th, Belov S P and Winnewisser G 1998 Precise measurement of the pure submillimeter-wave spectrum of HCl and DCl in their $v = 0$, 1 states *J. Mol. Spectrosc.* **187** 109–17
[44] Weiss C, Viehl E, Theiss Ch, Torosyan G, Weinacht M, Beigang R and Wallenstein R 2001 Einsatz breitbandiger THz-Strahlung in der Gasanalyse *Tech. Mess.* **68** 388–99
[45] Wagner Th Lecture on atmospheric remote sensing, IUP, University of Heidelberg, private communication
[46] Messer J K, De Lucia F C and Helminger P 1983 The pure rotational spectrum of water vapor—a millimeter, submillimeter, and far-infrared analysis *Int. J. Infrared Millim. Waves* **4** 505–39